Scattering suppression and confocal detection in multifocal multiphoton microscopy

Jörg Martini
Bielefeld University
Department of Physics
Experimental Biophysics and Applied Nanoscience
Universitätsstrasse 25
D-33615 Bielefeld, Germany
E-mail: jmartini@physik.uni-bielefeld.de

Volker Andresen
LaVision BioTec GmbH
Meisenstrasse 65
33607 Bielefeld, Germany

Dario Anselmetti
Bielefeld University
Department of Physics
Experimental Biophysics and Applied Nanoscience
Universitätsstrasse 25
33615 Bielefeld, Germany

Abstract. We have developed a new descanned parallel (32-fold) pinhole and photomultiplier detection array for multifocal multiphoton microscopy that effectively reduces the blurring effect originating from scattered fluorescence photons in strongly scattering biological media. With this method, we achieve a fourfold improvement in photon statistics for detecting ballistic photons and an increase in spatial resolution by 21% in the lateral and 35% in the axial direction compared to single-beam non-descanned multiphoton microscopy. The new detection concept has been applied to plant leaves and pollen grains to verify the improvements in imaging quality. [DOI: 10.1117/1.2736425]

Keywords: multiphoton processes; multiplexing; biomedical optics; stray light; confocal optics; microscopy.

Paper 06257R received Sep. 18, 2006; revised manuscript received Feb. 7, 2007; accepted for publication Mar. 2, 2007; published online May 15, 2007.

1 Introduction

Since its first experimental realization in 1990, multiphoton laser scanning microscopy (MPM)[1,2] has become an important tool for fluorescence and second harmonic generation (SHG) imaging.[3] Especially due to the advantageous use of near-infrared (NIR) excitation, which significantly reduces absorption and scattering, MPM is highly capable of deep tissue imaging.

However, relatively poor photon statistics due to small two-photon cross sections[2,4] of interesting fluorophores may be a concern for short acquisition times in MPM. In order to achieve sufficient fluorescence intensity at a given frame time and excitation power or to image dynamic processes with high frame rates at low excitation power, multibeam setups with microlenses,[5–7] diffractive optical elements,[8] or mirror beamsplitters[9,10] have been constructed, and large area real-time MPM to monitor biological dynamics[11–13] has been proven.

Single-beam excitation in combination with non-descanned PMT detection does not result in significant broadening of point spread functions,[14] although fluorescence or SHG photons are scattered inside the (biological) sample. In general, ballistic NIR multiphoton excitation generates fluorescence light in the focal volume inside the sample.[15] This light contributes to the unblurred image formation when reaching the detector, since both scattered and ballistic photons can be allocated to the excited focal volume. The limiting factor for deep tissue MPM imaging[16–18] is usually the loss of fluorescence light due to (multiple) scattering inside the sample.

Address all correspondence to Dipl. Phys. Jörg Martini, Bielefeld University, Experimental Biophysics, and Applied Nanoscience, Universitätsstr. 25 D-33615 Bielefeld, Germany; Tel: 49–521–1065392; Fax: 49–521–1062959; E-mail: jmartini@physik.uni-bielefeld.de

As single-beam non-descanned detection is a point-by-point scanning scheme, it may in practice require pixel dwell times in the range of μs, although high-speed MPM provides full frame imaging capability at video rate with corresponding pixel dwell times down to 100 ns (Refs. 19–21).

Multibeam setups, especially with non-descanned electron multiplying charge coupled device (EMCCD) cameras, which provide quantum efficiencies (Q.E.) up to 90%, also offer the advantage of video rate image acquisition. Due to their multiple-beam configuration and hence higher fluorescence yield, these setups are capable of imaging fluorophores of low brightness at high frame rates. However, image formation in this detection mode is affected by fluorescence photons that are scattered within the sample when they hit the CCD detector in an incorrect position. As a consequence, fluorescence images from deep optical planes within biological tissue are blurred as the ratio of scattered to ballistic fluorescence photons significantly increases. This implies that a non-descanned multibeam MPM loses its capability of generating three-dimensionally resolved fluorescence images deep inside the specimen, although sufficient fluorescence is excited and detected.

In this paper, we present a novel experimental setup that allows multifocal MPM imaging with good photon statistics and efficient suppression of scattered light by a descanned parallel (32-fold) pinhole and photomultiplier detection array. A four-fold improvement in photon statistics and an increase to a confocal[22,23] spatial resolution is shown in two-photon induced multifocal microscopy experiments on plant leaves and pollen grains.

1083-3668/2007/12(3)/034010/6/$25.00 © 2007 SPIE

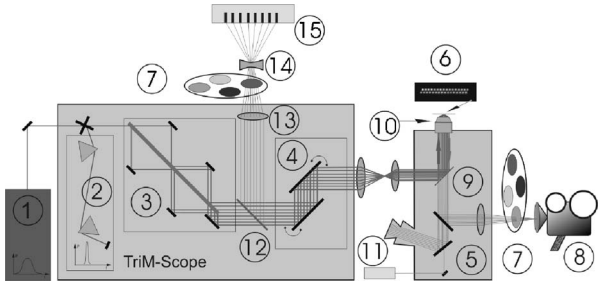

Fig. 1 Schematic experimental setup (see text for details).

2 Experimental Setup

The MPM consists of a mode-locked Tsunami Ti:Sa laser (Fig. 1, label 1), that is pumped by a Millenia X solid-state laser (both Spectra-Physics) and generates 100-fs laser pulses between 760 nm and 960 nm, a TriM-Scope (Fig. 1, labels 2 to 4) multi focal scanning unit (LaVision BioTec), and an inverted microscope (IX 71, Olympus, Fig. 1, label 5). The scanning unit contains an integrated pre-chirp section (Fig. 1, label 2) to compensate for laser pulse dispersion and two galvanometric mirror scanners (Fig. 1, label 4). The focus multiplexing section of the scanning unit (Fig. 1, label 3) splits the incident laser beam into a variable number of beams of the same average power. This section consists of a set of ten 100% reflective mirrors and one (adjustable) 50% mirror. By varying the position of the 50% mirror between the set of 100% mirrors, the laser beam can be split into 1, 2, $4, \ldots, 64$ beams, resulting in an adjustable number of excitation foci (Fig. 1, label 6) in the sample. In addition, laser power can be adjusted by a combination of two polarizers in order to achieve short acquisition times with sufficient fluorescence while keeping the photodamage minimal. A mechanical focus and sample drive (MFD, Märzhäuser) allows for the acquisition of depth-resolved fluorescence scans inside the sample. Data acquisition and experimental control is performed by the MPM's software package (Imspector, LaVision BioTec). Five-dimensional (5-D) fluorescent data sets (including spectral and temporal data axes) are handled and processed with Imspector, ImageJ,[24] or Imaris 4.0 (Bitplane AG) software packages.

Non-descanned detection of fluorescence is performed by a back-illuminated EMCCD camera (IXON BV887ECS-UVB, Andor Technology; Fig. 1, label 8) or a photomultiplier (H7422-40, Hamamatsu; Fig. 1, label 11) for a single exciting laser focus. The exciting NIR laser beams are directed via scan lens, tube lens, and dichroic mirror (2P-Beamsplitter 680 DCSPXR, Chroma, Fig. 1, label 9) onto the back aperture of the objective lens (UplanApo/IR, $60\times$/NA 1.2 W or XLUMPLFL20XW, NA 0.95 W, Olympus; Fig. 1, label 10) while stray light from the NIR in the detection path is blocked by a short pass filter (2P-Emitter E 700 SP, Chroma). In the descanned detection pathway, the dichroic mirror (Fig. 1, label 9) is replaced by a 100% silver-coated mirror and the exciting NIR and the fluorescence signal are separated by a dichroic beamsplitter (Fig. 1, label 12) between the mirror scanners and the beam multiplexing unit. Fluorescence is then directed through a short pass filter, two achromatic imaging lenses (both Linos, $f=300$ mm, Fig. 1, label 13, and $f=-50$ mm, Fig. 1, label 14) and a filter wheel (LaVision BioTec, Fig. 1, label 7) and imaged onto a home-built pinhole array (0.5-mm-thick aluminum board with drilled pinholes) in front of the detecting 32-fold multi-anode PMT (H7260-01, Hamamatsu; Fig. 1, label 15). The complete imaging optics (objective lens, scan and tube lens, and two imaging lenses) in descanned detection defines a magnification of 1880-fold for the $60\times$ objective lens and 627-fold for the $20\times$ objective lens, respectively. The photon flux on individual PMT segments is detected by a home-built 32-fold integration amplifier and sampled by a multiplexed multichannel AD-conversion board (DAQ2204, Adlink). Later we present some detailed aspects of our experimental setup that are helpful for an in-depth understanding of image formation in parallel descanned detection.

It is worth noting that in descanned detection, no complete image of the sample is generated. The fluorescence intensities generated by the laser foci remain stationary on their corresponding detection pinholes, as excitation NIR and fluorescence light are led through the same optical path via the scanning mirrors, hence the term "descanned." To generate images, fluorescence intensity has to be correlated with the scanning mirror positions at the moment of AD-sampling. Furthermore, in parallel detection, 32 images of slightly shifted sample regions are generated, each excited by its corresponding laser focus. In this paper, we present results that use the 32-fold overlapping region as the region of interest in the sample. The shift in relative position of the individual images is due to the fact that individual fluorescent foci in the sample are separated from each other (for a given scanning mirror position, they form a zigzag line with a length of 17 μm for the $60\times$ objective lens and 51 μm for the $20\times$ objective lens), and therefore correlation of fluorescence intensity with mirror position reveals different sample regions. After defining a shift vector for each channel that is dependent on the step width of the scanning mirrors, the individual pixel values of the 32 images are added up with respect to the shift vector by an ImageJ macro. To properly align these different images, their size is doubled (e.g., 300×300 pixels to 600×600 pixels) before adding so that the pixelation of the final image is four times smaller than in the original images. This doubling helps to manually align the 32 sample regions when defining the shift vectors. When imaging fluorescent beads, the standard procedure for image alignment, an individual bead might, for example, cover 1×1 pixel in one image and 1×2 pixels in another image. For their doubled sizes, these beads can be aligned centered. Currently, the sampling rate of the AD-conversion board (max. 90 kHz for 32 channels, e.g., resulting in one 300×300 pixels per second image) is the practical limitation for frame speed in our setup.

3 Results and Discussion

3.1 *Stray Light Suppression*

Non-descanned camera detection in multifocal multiphoton microscopy offers the advantage of excellent fluorescence photon statistics, as many excitation foci contribute to the generation of a fluorescence image, while excitation energy remains below the damage threshold of the sample. However, when fluorescence light is generated in deep optical planes inside the sample, it can be scattered on its detection path

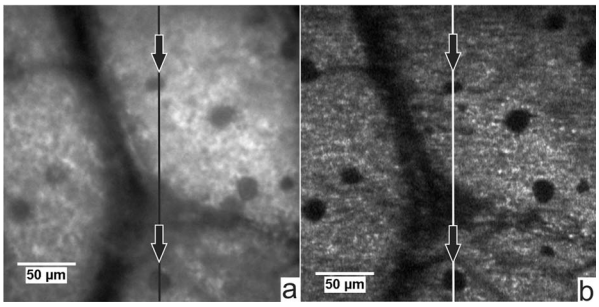

Fig. 2 Multifocal two-photon (800-nm) excited autofluorescence of *Ficus benjamini* leaf 45 μm inside the sample in minimum-maximum representation: (a) non-descanned camera detection; (b) 32-fold parallel descanned detection.

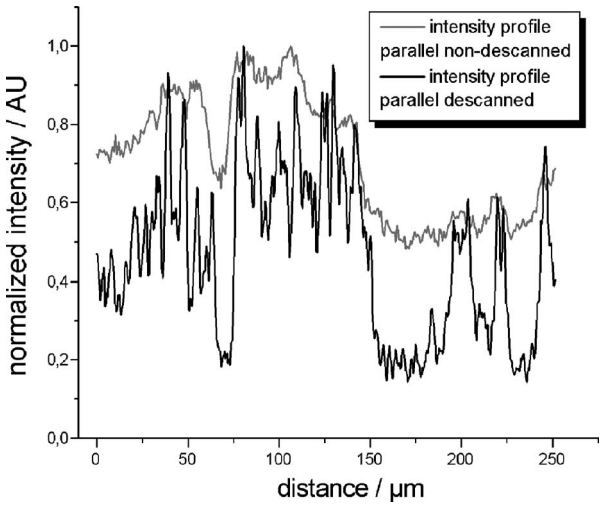

Fig. 3 Fluorescence intensity profile along vertical lines in Fig. 2.

within the sample. A high ratio of ballistic to scattered fluorescence photons is crucial for crisp non-descanned camera images, as scattered photons are responsible for image haze, which eventually can mask faint sample details.

In our parallel descanned concept, scattered fluorescence is blocked by detection pinholes, allowing only ballistic photons to reach the PMT segments. Figure 2 shows two-photon induced autofluorescence images of the identical optical plane 45 μm inside a *Ficus benjamini* leaf and provides a typical example of the blur effects described earlier. Whereas Fig. 2(a) has been taken in non-descanned camera detection, Fig. 2(b) was measured in parallel descanned detection mode, using 0.4-mm-diam detection pinholes for optimal scattered fluorescence light suppression. In order to quantify the gain in contrast, two vertical intensity profiles (Fig. 3) have been extracted from both images, as indicated by the two lines in Fig. 2. Both profiles have been normalized to show the actual image dynamics. From the profiles in Fig. 3, it is evident that the parallel descanned detection image [Fig. 2(b)] yields a higher pixel dynamics (i.e., granular chloroplasts), a larger absolute minimum-maximum ratio, and steeper edge slopes at large, distinct image features. (Note the two organelles in Fig. 2 indicated by arrows and their corresponding fluorescence intensities located at 70 to 75 μm and at 225 to 240 μm in Fig. 3.)

In conclusion, descanned detection in combination with pinholes sufficiently suppresses sample scattered fluorescence and therefore allows high-contrast multifocal induced fluorescence imaging of deep[25] optical planes. However, this is achieved by blocking unwanted fluorescence light so that the absolute fluorescence intensity is generally much lower than compared to high Q.E. CCD cameras. It is interesting to note that the depth limitation of this imaging concept is determined by the complete loss of ballistic fluorescence signal and not by the ratio of scattered to ballistic photons as in non-descanned camera detection (see Fig. 2).

Table 1 Comparison of point spread functions of fluorescent beads (diam 175 nm, emission maximum 515 nm, two-photon excitation 800 nm, NA 1.2, n=1.33).

Detection	FWHM	Resolution
Confocal parallel descanned axial	618 nm±25.5 nm	735 nm±30.3 nm
Confocal parallel descanned lateral	266.1 nm±17.1 nm	316.4 nm±20.4 nm
Single-beam non-descanned PMT detection axial	943.8 nm±53.4 nm	1122.2 nm±63.5 nm
Single-beam non-descanned PMT detection lateral	337.3 nm±33.6 nm	401 nm±40 nm
Theoretical two-photon excitation axial	887.8 nm	1055.6 nm
Theoretical two-photon excitation lateral	313.2 nm	372.4 nm
Theoretical two-photon excitation, confocal detection axial	602.6 nm	716.5 nm
Theoretical two-photon excitation, confocal detection lateral	211.9 nm	252 nm

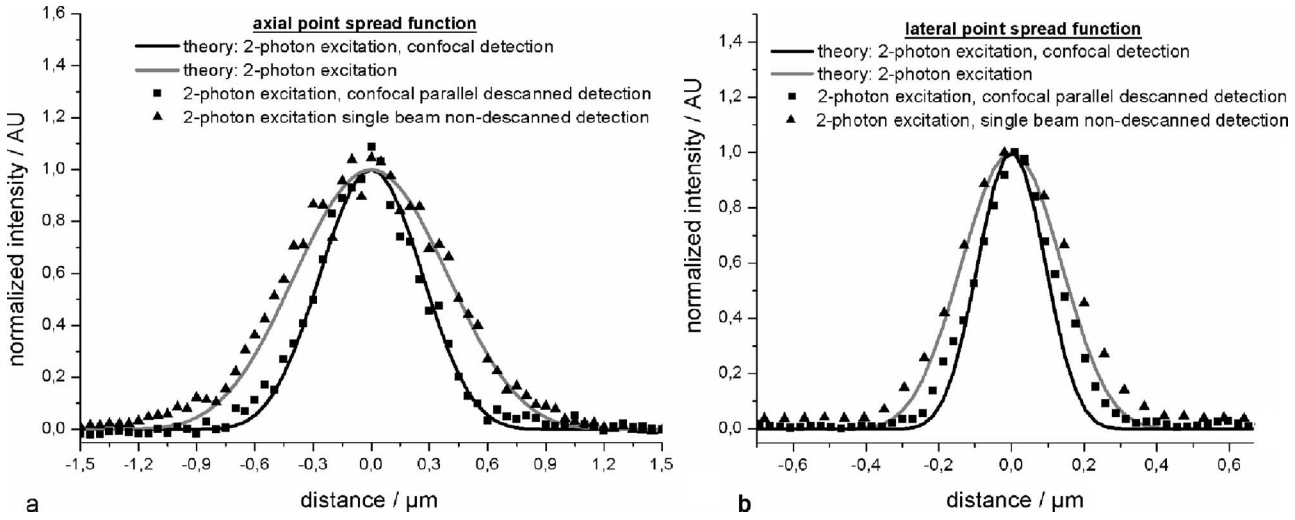

Fig. 4 Axial (a) and lateral (b) point spread functions, theoretical curves calculated for high aperture objective lens[27,28] (NA 1.2), experimental PSF measured with two-photon excitation (800 nm) of fluorescent beads (emission maximum 515 nm) in water (refractive index n=1.33).

3.2 *Multiphoton Confocal Detection*

In order to measure point spread functions (PSFs), we have imaged fluorescent beads with a diameter below the instrument's resolution (FluoSpheres 505/515, Invitrogen, d=175 nm) that have been immobilized on a glass coverslip and submerged in water. Special care has been taken to properly adjust the coverslip correction of the UplanApo objective lens. In the confocal parallel descanned detection, the pinhole size was set to 0.4 mm, significantly smaller than the magnified diameter of the airy disk for a 515-nm point source (d=0.985 mm) to ensure comparability with the theoretical values calculated in Table 1. Typical results of these measurements are presented in Fig. 4. Both axial and lateral PSFs of the confocal parallel descanned detection clearly show improved full width at half maximum (FWHM) when compared to a theoretical two-photon excitation PSF as well as to an experimental PSF in the non-descanned detection mode. Measurement data have been fitted to a Gauss profile,[26] and their FWHM has been calculated from the Gauss fit. The optical resolutions have been calculated for an emission wavelength of 515 nm, assuming Gauss profiles and applying the Rayleigh criterion (contrast 26.4%). The corresponding numbers are listed in Table 1. From Table 1, it can be concluded that experimental and corresponding theoretical FWHM values match very well. Therefore, in this measurement configuration (excitation: 800 nm; emission: 515 nm; NA: 1.2; and refractive index: 1.33), axial and lateral resolutions of the confocal parallel non-descanned detection mode are improved by 35% and 21% (theoretically possible: 36% and 37%), respectively, compared to the non-descanned PMT detection mode. This improvement to 735 nm (theoretical: 716.5 nm) in the axial and to 316.4 nm (theoretical: 255 nm) in the lateral case is due to the use of pointlike detectors rather than finite-size detectors, which to our best knowledge has not been experimentally implemented in multifocal or line scanning setups to date. The slight broadening of the PSFs' experimental values in comparison to the theoretical ones is probably due to imperfect overfilling of the back aperture of the objective lens, aberrations in the magnifying optics in the parallel confocal detection case, and imperfect image shift vectors, which especially effect lateral PSFs.

To demonstrate the resolution improvements, we performed three-dimensional (3-D) fluorescence measurements of a fixed pollen sample. Especially when examining optical planes above the massive core body of the pollen (see Fig. 5), improved resolution of the confocal parallel descanned detec-

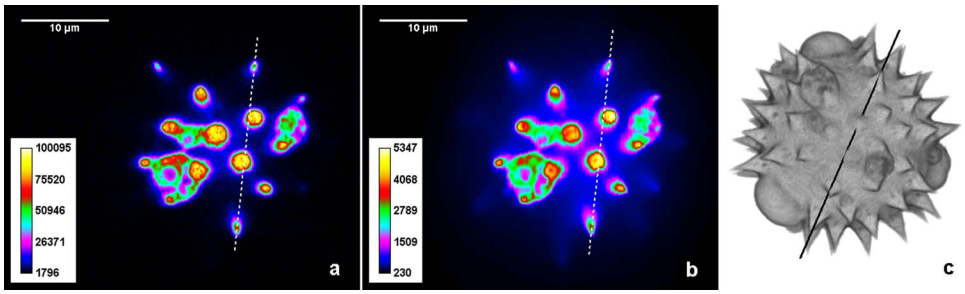

Fig. 5 Two-photon (800-nm) excited fluorescence of pollen. Optical planes (a) and (b) are located 1.5 μm above the massive central pollen body; spikes of pollen penetrate the optical plane. The dashed line indicates the direction of the profile in (a) confocal parallel descanned detection and (b) single beam non-descanned detection. (c) Voxel representation of complete 3-D confocal parallel descanned detection dataset; black line indicates the direction of the profiles in Fig. 6.

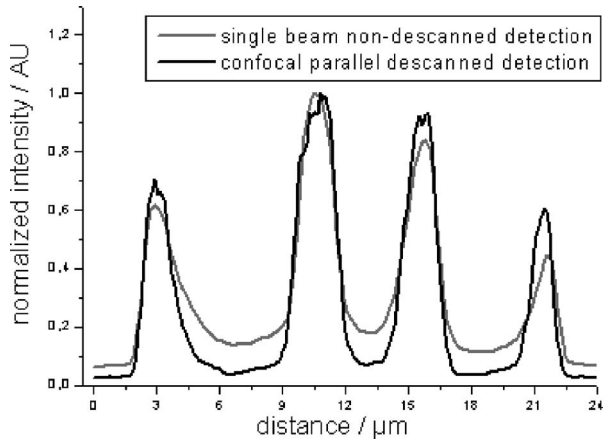

Fig. 6 Normalized fluorescence intensity profiles of pollen as indicated in Fig. 5. Note the higher minimum-maximum ratio and the steeper slopes in the confocal parallel descanned detection mode.

tion became apparent: while the non-descanned detection mode [Fig. 5(b)] suffers from significant fluorescent background of the pollen body, the confocal parallel descanned detection filters out this background due to its improved z-resolution. This becomes obvious when comparing the two normalized intensity profiles in Fig. 6, which have been derived from the fluorescence intensity data presented in Fig. 5(a) and 5(b). For the confocal parallel descanned detection mode in this measurement, fluorescence signal-to-noise and signal-to-background are improved by 200% and up to 350%, respectively.

3.3 *Detection Efficiency*

In order to quantify improvements in the photon statistics, we measured fluorescence intensities of 1 mM Rhodamin 6G dissolved in water in descanned and non-descanned detection modes upon using the identical detector (H-7422-40) and experimental parameters (60× objective lens, acquisition time, laser power, etc.). In both cases, detection efficiencies are similar when placing the detector in the focal plane of the first (f=300 mm) imaging lens, resulting in a 360-fold magnification of the exciting focus, which means that descanned detection in our setup does not result in a loss of signal intensity for ballistic photons.

When comparing descanned detection between the previously mentioned 360-fold magnification and the necessary 1880-fold (627-fold for the 20× objective lens) magnification, we measured a loss in signal of approximately 23% with the multi-anode PMT (H7260-01) for a single beam. This loss is due to aberrations in the magnifying optics that image outside the active detection area (0.8 mm × 8 mm) of the PMT. Further losses in fluorescence intensity occur when introducing the pinhole array in front of the PMT, i.e., a total loss of a factor of 4 for pinholes with a diameter of 0.8 mm. These losses are reciprocally dependent on the size of the pinholes. However, pinholes are necessary to block out scattered light from all the other fluorescent foci. This means that choosing a particular set of pinholes is a trade-off between signal intensity and suppression of scattered light. Therefore, it is also possible to choose pinholes with a larger diameter (e.g., 1 mm), which would increase the throughput significantly at the expense of resolution but still keep a comparable level of scattering suppression.

Furthermore, when comparing parallel descanned detection to single-beam non-descanned detection, it has to be noted that the high-efficiency H-7422-40 PMT single-beam detector's Q.E. is roughly twice the Q.E. of the H7260-01 multi-anode PMT.

Therefore, the advantage of the 32-fold generation of fluorescence intensity in parallel descanned detection with 0.8-mm-diam pinholes and the 60× objective lens is compromised by a factor of 8 (factor 4 due to pinhole blocking and factor 2 due to Q.E.). This results in a four-fold increase in photon statistics for ballistic photons in parallel descanned detection compared to non-descanned single-beam detection.

The efficiency for the two detection methods can be compared when assuming that the detected fluorescence intensity $\mathbf{I_{sb}}=\mathbf{I_s}+\mathbf{I_b}$ for non-descanned single-beam detection is composed of all scattered $\mathbf{I_s}$ and ballistic $\mathbf{I_b}$ fluorescence light, while the detected fluorescence intensity $\mathbf{I_{pd}}$ for parallel descanned beam detection was measured to be $\mathbf{I_{pd}}=4\cdot\mathbf{I_b}$. Hence, parallel descanned detection provides better photon statistics than non-descanned single-beam detection, as long as the ratio of scattered to ballistic photons remains smaller than a factor of 3.

Due to the higher Q.E. of the single-beam detector and losses due to the pinholes for parallel descanned detection, single-beam non-descanned detection is more appropriate for weak fluorescence applications, when the signal-to-noise ratio becomes the limiting factor of the measurement. Furthermore, this detection method is relatively insensitive to scattered fluorescence, so especially low fluorescence detection in scattering samples is best performed by non-descanned single-beam detection.

Therefore, one can conclude that parallel descanned detection is best suited for samples with a relatively high fluorescence level so that blocking of scattered fluorescence from deep imaging planes does not result in a complete loss of signal. In this operative range, parallel descanned detection has advantages over both single-beam non-descanned detection, because of improved photon statistics, which can be utilized to reduce image acquisition time, and multibeam non-descanned camera detection, because of drastically reduced scattering haze.

4 Conclusion

In conclusion, the obtained results show that parallel descanned detection in multifocal multiphoton microscopy with our novel parallel 32-fold pinhole and PMT array can be applied to image thick biological tissues. Imaging of pollen grains and plant leaves exhibited improved photon statistics and multifocal multiphoton induced confocal resolution. As a consequence, it will be possible to observe dynamic processes at certain depths inside the sample with significantly higher temporal resolution than has been achieved up to now. In this way, the parallel descanned method represents a promising instrumentation for microscopy applications in life sciences and biophotonics.

Acknowledgments

We thank H. Spiecker, K. Schröder, K. Tönsing, C. Pelargus, R. Eckel, and K. Schnurrbusch for valuable discussions and for technical and mathematical support. Financial support from BMBF in the Biophotonics Research Initiative (Grant MEMO, FKZ: 13N8432) is gratefully acknowledged.

References

1. W. Denk, J. H. Strickler, and W. W. Webb, "Two-photon laser scanning fluorescence microscopy," *Science* **248**, 73–76 (1990).
2. W. R. Zipfel, R. M. Williams, R. Christie, A. Y. Nikitin, B. T. Hyman, and W. W. Webb, "Live tissue intrinsic emission microscopy using multiphoton-excited native fluorescence and second harmonic generation," *Proc. Natl. Acad. Sci. U.S.A.* **100**, 12, 7075–7080 (2003).
3. P. J. Campagnola and L. M. Loew, "Second-harmonic generation imaging microscopy for visualizing biomolecular arrays in cells, tissues, and organisms," *Nat. Biotechnol.* **21**, 1356–1360 (2003).
4. A. A. Albota, C. Xu, and W. W. Webb, "Two-photon fluorescence excitation cross sections of biomolecular probes from 690 to 960 nm," *Appl. Opt.* **37**(31), 7352–7356 (1998).
5. A. H. Buist, M. Müller, J. Squier, and G. J. Brakenhoff, "Real time two-photon absorption microscopy using multi-point excitation," *J. Microsc.* **192**(Pt. 2), 217–226 (1998).
6. A. Egner, V. Andresen, and S. W. Hell, "Comparison of the axial resolution of practical Nipkow-disk confocal fluorescence microscopy with that of multifocal multiphoton microscopy: theory and experiment," *J. Microsc.* **206**(Pt. 1), 24–32 (2002).
7. J. Bewersdorf, R. Pick, and S. Hell, "Multifocal multiphoton microscopy," *Opt. Lett.* **23**(9), 655–657 (1998).
8. L. Sacconi, E. Froner, R. Antolini, M. R. Taghizadeh, A. Choudhury, and F. S. Pavone, "Multiphoton multifocal microscopy exploiting a diffractive optical element," *Opt. Lett.* **28**(20), 1918-1920 (2003).
9. T. Nielsen, M. Fricke, D. Hellweg, and P. Andresen, "High efficiency beam splitter for multifocal multiphoton microscopy," *J. Microsc.* **201**(3), 368–376 (2001).
10. D. N. Fittinghoff, P. W. Wiseman, and J. A. Squier, "Widefield multiphoton and temporally decorrelated multifocal multiphoton microscopy," *Opt. Express* **7**(8), 273–279 (2000).
11. J. Kalb, T. Nielsen, M. Fricke, M. Egelhaaf, and R. Kurtz, "*In vivo* two-photon laser-scanning microscopy of Ca2+ dynamics in visual motion-sensitive neurons," *Biochem. Biophys. Res. Commun.* **316**(2), 341–347 (2004).
12. R. Kurtz, M. Fricke, J. Kalb, P. Tinnefeld, and M. Sauer, "Application of multiline two-photon microscopy to functional *in vivo* imaging," *J. Neurosci. Methods* **151**(2), 276–286 (2006).
13. R. Tyzio, R. Cossart, I. Khalilov, M. Minlebaev, C. A. Hubner, A. Represa, Y. Ben Ari, and R. Khazipov, "Maternal oxytocin triggers a transient inhibitory switch in GABA signaling in the fetal brain during delivery," *Science* **314**(5806), 1788–1792 (2006).
14. C. Y. Dong, K. Koenig, and P. So, "Characterizing point spread functions of two-photon fluorescence microscopy in turbid medium," *J. Biomed. Opt.* **8**(3), 450–459 (2003).
15. H. Szmacinski, I. Gryczynski, and J. R. Lakowicz, "Spatially localized ballistic two-photon excitation in scattering media," *Biospectroscopy* **4**(5), 303–310 (1998).
16. F. Helmchen and W. Denk, "Deep tissue two-photon microscopy," *Nat. Methods* **2**(12), 932–940 (2005).
17. E. Beaurepaire, M. Oheim, and J. Mertz, "Ultra-deep two-photon fluorescence excitation in turbid media," *Opt. Commun.* **188**(1–4), 25–29 (2001).
18. X. S. Gan and M. Gu, "Fluorescence microscopic imaging through tissue-like turbid media," *J. Appl. Phys.* **87**, 7, 3214–3221 (2000).
19. K. H. Kim, C. Buehler, and P. T. C. So, "High-speed two-photon scanning microscope," *Appl. Opt.* **38**(28), 6004–6009 (1999).
20. R. D. Roorda, T. M. Hohl, R. Toledo-Crow, and G. Miesenbock, "Video-rate nonlinear microscopy of neuronal membrane dynamics with genetically encoded probes," *J. Neurophysiol.* **92**, 1, 609–621 (2004).
21. G. Y. Fan, H. Fujisaki, A. Miyawaki, R. K. Tsay, R. Y. Tsien, and M. H. Ellisman, "Video-rate scanning two-photon excitation fluorescence microscopy and ratio imaging with cameleons," *Biophys. J.* **76**(5), 2412–2420 (1999).
22. R. Gauderon, P. B. Lukins, and C. J. Sheppard, "Effect of a confocal pinhole in two-photon microscopy," *Microsc. Res. Tech.* **47**(3), 210–214 (1999).
23. E. H. K. Stelzer, S. Hell, S. Lindek, R. Stricker, R. Pick, C. Storz, G. Ritter, and N. Salmon, "Nonlinear absorption extends confocal fluorescence microscopy into the ultra-violet regime and confines the illumination volume," *Opt. Commun.* **104**(4–6), 223–228 (1994).
24. W. S. Rasband, "ImageJ," http://rsb.info.nih.gov/ij/, US. National Institutes of Health, Bethesda, MD (1997).
25. V. E. Centonze and J. G. White, "Multiphoton excitation provides optical sections from deeper within scattering specimens than confocal imaging," *Biophys. J.* **75**(4), 2015–2024 (1998).
26. W. R. Zipfel, R. M. Williams, and W. W. Webb, "Nonlinear magic: multiphoton microscopy in the biosciences," *Nat. Biotechnol.* **21**, 1369–1377 (2003).
27. C. J. R. Sheppard and H. J. Matthews, "Imaging in high-aperture optical-systems," *J. Opt. Soc. Am. A* **4**, 8, 1354–1360 (1987).
28. M. Gu, *Principles of Three-Dimensional Imaging in Confocal Microscopes*, World Scientific Publishing, Singapore (1996).